Geoscience Frontiers xxx (2013) 1–14

Contents lists available at ScienceDirect

China University of Geosciences (Beijing)

Geoscience Frontiers

journal homepage: www.elsevier.com/locate/gsf

Research paper

Fault on–off versus coseismic fluids reaction

C. Doglioni [a,c,*], S. Barba [b], E. Carminati [a,c], F. Riguzzi [b]

[a] Dipartimento di Scienze della Terra, Università Sapienza, Roma, Italy
[b] Istituto Nazionale di Geofisica e Vulcanologia, Roma, Italy
[c] Istituto di Geologia Ambientale e Geoingegneria, CNR, Roma, Italy

ARTICLE INFO

Article history:
Received 9 July 2013
Received in revised form
14 August 2013
Accepted 16 August 2013
Available online xxx

Keywords:
Fault activation
Brittle-ductile transition
Earthquake
Fluids response

ABSTRACT

The fault activation (fault on) interrupts the enduring fault locking (fault off) and marks the end of a seismic cycle in which the brittle-ductile transition (BDT) acts as a sort of switch. We suggest that the fluid flow rates differ during the different periods of the seismic cycle (interseismic, pre-seismic, coseismic and post-seismic) and in particular as a function of the tectonic style. Regional examples indicate that tectonic-related fluids anomalies depend on the stage of the tectonic cycle and the tectonic style. Although it is difficult to model an increasing permeability with depth and several BDT transitions plus independent acquicludes may occur in the crust, we devised the simplest numerical model of a fault constantly shearing in the ductile deeper crust while being locked in the brittle shallow layer, with variable homogeneous permeabilities. The results indicate different behaviors in the three main tectonic settings. In tensional tectonics, a stretched band antithetic to the normal fault forms above the BDT during the interseismic period. Fractures close and fluids are expelled during the coseismic stage. The mechanism reverses in compressional tectonics. During the interseismic stage, an over-compressed band forms above the BDT. The band dilates while rebounding in the coseismic stage and attracts fluids locally. At the tip lines along strike-slip faults, two couples of subvertical bands show different behavior, one in dilation/compression and one in compression/dilation. This deformation pattern inverts during the coseismic stage. Sometimes a pre-seismic stage in which fluids start moving may be observed and could potentially become a precursor.

1. Introduction

The seismic cycle consists of a long interseismic period (the fault "off" state) followed by almost instantaneous coseismic and possibly longer postseismic periods (the fault "on" state; e.g., Thatcher and Rundle, 1979; Savage, 1983; Cattin and Avouac, 2000; Meade and Hager, 2005; Sieh et al., 2008). The locking of a fault and the earthquake generation depend on a variety of factors. These include the rate- and state-dependent instability underlying true stick-slip behavior (the Dietrich-Ruina model, Ruina, 1983; Marone, 1998), the elasto-plastic instabilities (Hobbs and Ord, 1988), the thickness and composition of the elastic layer (Thatcher, 1993), and the failure of asperities (Kanamori and Anderson, 1975) or other irregularities along the fault surface. The need for improved earthquake hazard analysis procedures, both for probabilistic and neo-deterministic approaches, calls for better understanding of the seismic cycle (Peresan et al., 2005; Slejko et al., 2010; Panza et al., 2012; Peresan and Panza, 2012). Fluid variations, in terms of chemical and flux rates, are sensitive to the seismic cycle (e.g., Sibson, 1992) and may depend on the tectonic style (Muir-Wood and King, 1993). We consider the partitioning of strain between brittle and ductile structural levels as one of the mechanisms controlling the seismic cycle which was proposed in Doglioni et al. (2011). Based on this simplified geological and numerical model of a two-layer crust with a single brittle-ductile transition (BDT) that links the ongoing ductile deformation at depth with the fragile episodic behavior in the upper crust, here we analyze the different reaction of fluids as a function of the tectonic style. For

* Corresponding author. Dipartimento di Scienze della Terra, Università Sapienza, Roma, Italy.
E-mail address: carlo.doglioni@uniroma1.it (C. Doglioni).

Peer-review under responsibility of China University of Geosciences (Beijing)

Production and hosting by Elsevier

1674-9871/$ – see front matter © 2013, China University of Geosciences (Beijing) and Peking University. Production and hosting by Elsevier B.V. All rights reserved.
http://dx.doi.org/10.1016/j.gsf.2013.08.004

sake of simplicity, we hypothesize straight fault planes for the three main tectonic settings (extensional, contractional, transcurrent), being aware that in nature they rather undulate and may be listric. At the transition between the ductile steady-state deformation along a shear zone in metamorphic environment, and the overlying brittle episodic fault plane, we speculate that different porosity develops. Along a normal fault, from the BDT upward, a dilated band forms in the hangingwall (Fig. 1). Along a reverse fault or thrust it rather forms an over-compressed band (Fig. 1). In a strike-slip setting, from the BDT upward, different bands should occur at the tip lines of the locked fault, both in contraction and in dilation (Fig. 2).

2. Role and behavior of fluids

Many researchers have recognized that fluids are crucial in fault mechanics and a rather vast literature is growing on the relation between seismicity and hydrology (Bodvarsson, 1970; Sibson, 1981, 1992; Cox, 1995; Miller et al., 1996; Miller and Nur, 2000; Miller, 2002; Tenthorey et al., 2003; Micklethwaite and Cox, 2004; Manga and Wang, 2007). The active role of fluids in decreasing fault strength is certainly relevant for the mechanics of the fault behavior and cyclic activation. Fluid overpressure should develop at the beginning of the coseismic stage. This mechanism should be self-supporting. As the fluid pressure increases, e.g., because of the initial subsidence of the hangingwall of a normal fault, the fault strength decreases, thus favoring the initial motion of the hangingwall. This will further increase pore pressure, eventually favoring the nucleation of the mainshock. Pore pressure variation can explain the increase or decrease of the water table and the variations in the chemical composition of fluids, which have often been observed during earthquakes (e.g., Manga and Wang, 2007). The permeability and fluid diffusion into rock voids depend on the primary texture and porosity, the fracture width and the degree of connectivity, which control secondary porosity. Fault planes may represent preferential conduits or even barriers for fluids, e.g., an impermeable formation becomes permeable when faulted, and vice versa a permeable rock when finely cataclastically brecciated may become impermeable. Moreover, as a function of the involved lithology and the diffusion of fractures, the faults may have focused channeling of fluids (Eichhubl and Boles, 2000). Therefore, the original lithology plays a fundamental role apart from the roles mentioned in this paper. Crustal ruptures may induce a fault-valve behavior, involving cyclic accumulation and a release of fluids (Sibson, 1992). Variations in fluid flux have been observed during seismic sequences (e.g., Rudnicki et al., 1993). Therefore, fluid (e.g., H_2O, CO_2, Rn) discharge patterns may be a relevant parameter in short-term earthquake hazard assessment. Radon variations and water level in wells have been suggested to be reliable precursors in Japan (Wakita, 1996). Because an increase of fluid pore pressure decreases the fault strength, its variation in time may control the episodic activity of faults. Fluids may actively trigger fault ruptures along asperities (Miller et al., 2004), as discussed in Matthäi and Fischer (1996). However, fluids also have a relevant passive role (e.g., Tullis et al., 1996; Wannamaker et al., 2002). In fact, fluids are squeezed by pressure gradients and are transported depending on rock permeability (Salazar et al., 2002). Metamorphic phase transitions and shear in the lower crust can also provide fluids that are delivered upward (Tullis et al., 1996). Wherever the fluids originate, e.g., in the surface (meteoric) or at various depths in the crust or mantle (from magmatic and metamorphic reactions), they move when a variation in the state of stress occurs. According to Sibson et al. (1975), a consequence of the dilatancy/fluid-diffusion mechanism for shallow earthquakes is that considerable volumes of fluid are rapidly redistributed in the crust following seismic faulting. This is borne out by the outpourings of warm groundwater, which

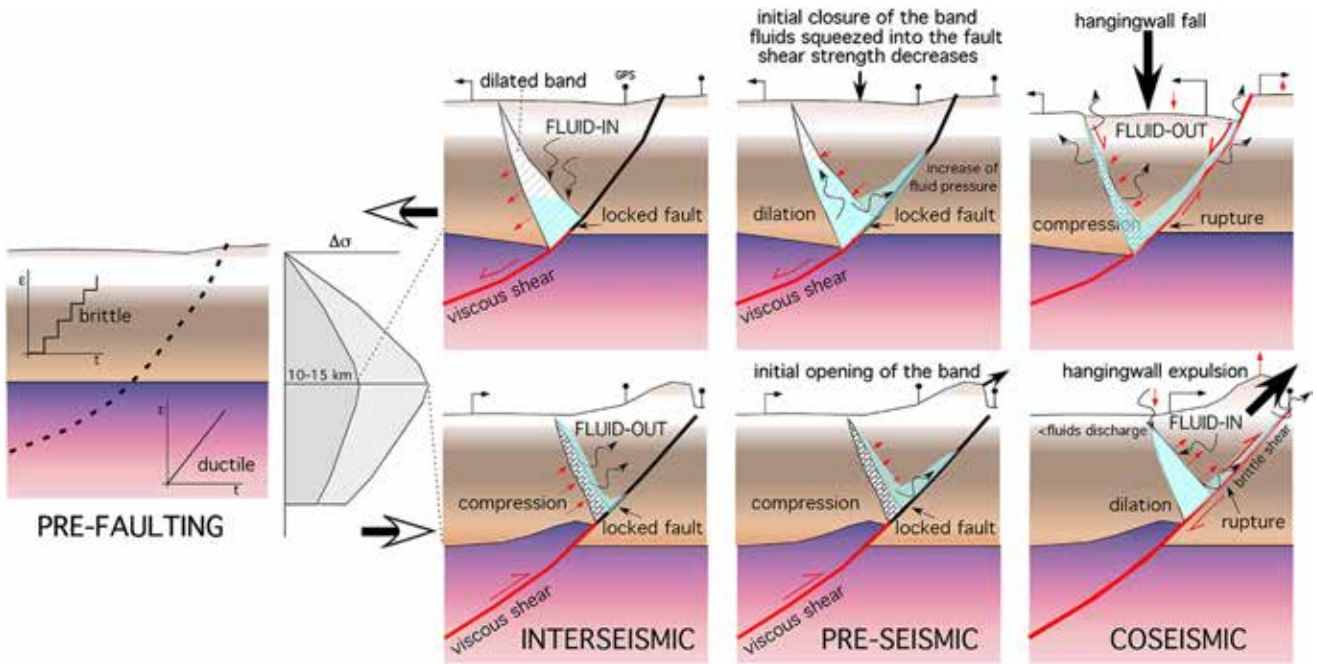

Figure 1. Assuming a simplified two-layer crustal rheology, the ductile lower crust is characterized by a constant strain rate whereas the brittle upper crust displays episodic locking-unlocking behavior. Tensional and compressional faults generate opposite kinematics and mechanical evolutions. In the tensional tectonic environment, the triangle of crust above the BDT remains "suspended" while a dilated area forms during the interseismic period. Fluids may enter the fractured volume. Once shear stress along the locked part of the fault becomes larger than fault strength, the hangingwall will begin to collapse, increasing the fluid pressure into the fault gouge. This mechanism is self-supporting because it decreases fault strength, facilitating the final fall of the hangingwall generating the mainshock. Conversely, during the interseismic period, along a thrust plane an over-compressed band separates the ductile shear from the overlying locked fault segment. The hangingwall is eventually expelled during the coseismic period. Fluids discharge behaves differently as a function of the tectonic field.

Please cite this article in press as: Doglioni, C., et al., Fault on–off versus coseismic fluids reaction, Geoscience Frontiers (2013), http://dx.doi.org/10.1016/j.gsf.2013.08.004

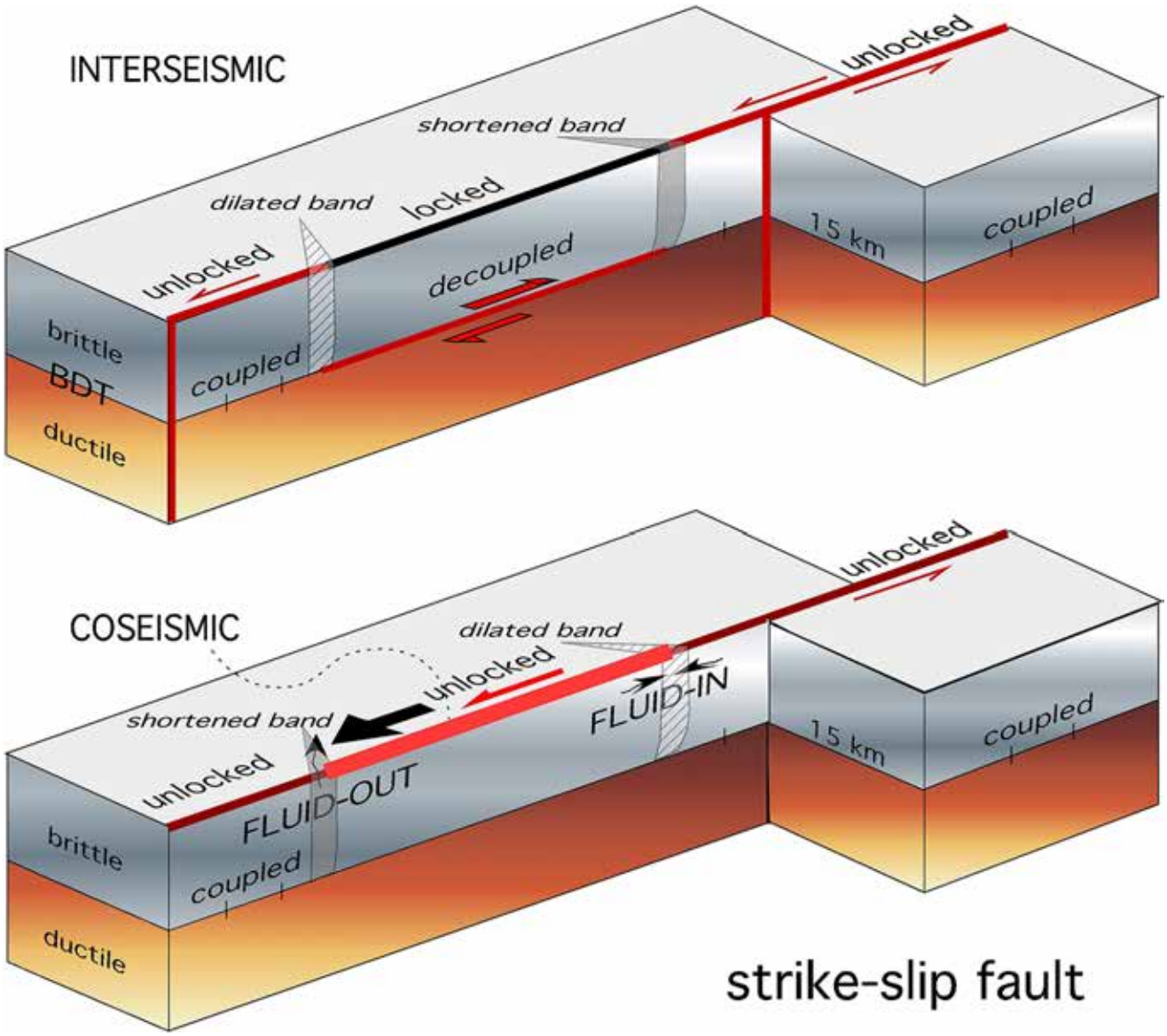

Figure 2. An interseismic and coseismic model for an ideal strike-slip fault crossing the BDT. Along the locked brittle part of the fault, basal shear with the ductile lower crust is inferred, and two bands with opposite evolution (tension and shortening) form at the tip points of the inactive part of the fault. Strike-slip faults may have coexisting, locked and unlocked (creeping) segments. Along the unlocked segments of the fault, the brittle layer rather moves coherently with the deeper ductile layer. During the coseismic stage, the locked fault moves instantaneously, temporarily reversing the strain in the two bands, e.g., the dilated band is shortened. The overcompressed band is however rather dilated. During the coseismic stage, fluids are squeezed out in the shortened band, and the opposite behavior is expected along the dilated band.

have been observed along fault traces following some moderate (M 5–M 7) earthquakes (Sibson et al., 1975). The quantities of fluid involved are such that significant hydrothermal mineralization may result from each seismically induced fluid pulse, and the mechanism provides an explanation for the textures of hydrothermal vein deposits associated with ancient faults, which almost invariably indicate that mineralization was episodic (Sibson et al., 1975). It has also been demonstrated that the size of water fluctuation in a given well is related to the magnitude of each earthquake, and the distance form the well (Matsumoto and Takahashi, 1994; Roeloffs, 1998).

Moreover, fluid discharges of the opposite sign, i.e., positive and negative during the coseismic period, have been inferred along normal faults and thrusts, respectively (e.g., Muir-Wood and King, 1993). However, in spite of this important issue, which may be relevant for discriminating useful seismic precursors (Roeloffs, 1988; Roeloffs and Quilty, 1997), not many studies have tried to classify variations in fluids discharge or depth of the water table as a function of the type of fault. Therefore, following the tectonic model of Fig. 1, we try to further investigate how (i) the style of faulting could determine fluids discharge (either positive or negative), and how (ii) the lateral variations from the hypocenter/epicenter of the stress field both during the interseismic and coseismic stages, provide stress gradients which may increase and decrease porosity and the inversely related fluid discharge, even along the same activated fault.

3. Regional examples

We list below few of the several examples described in the literature about the role and the reaction of fluids with respect to seismic events.

Please cite this article in press as: Doglioni, C., et al., Fault on–off versus coseismic fluids reaction, Geoscience Frontiers (2013), http://dx.doi.org/10.1016/j.gsf.2013.08.004

3.1. Normal faults versus fluids

An increase in fluid expulsion during the activation of normal faults has been suggested (e.g., Sibson, 2000). The 1997–1998 normal fault-related seismic sequence of Umbria-Marche (Northern Apennines, Italy) presented a coseismic increase of fluid flux, but during the later interseismic period, the flux returned to lower values (Italiano et al., 2009). A similar increase of fluid discharge was observed in the 1980 Irpinia normal fault-related event (Pingue and De Natale, 1993). The L'Aquila April 6, 2009 event modified hydrological underground circulation on a large scale. The groundwater table rose significantly, and water discharge increased during the mainshock far from the epicentral area (Adinolfi et al., 2009; Amoruso et al., 2011). Approximately three hours after the mainshock, the fluid flux increased within a short time from 460 to nearly 570 L/s and remained stable for several weeks after a limited period of overflow (Fig. 3). Uranium emissions also increased in the months predating the earthquake (Plastino et al., 2011). Fluid overpressure close to the hypocenter was proposed for the L'Aquila 2009 earthquake (Di Luccio et al., 2010; Lucente et al., 2010; Terakawa et al., 2010). The V_P/V_S increased progressively from October 2008 to the April 6, 2009 mainshock because of an increase in pore fluid pressure along the NW-SE striking fault planes (Lucente et al., 2010; Terakawa et al., 2010). Di Luccio et al. (2010) proposed a hydraulic diffusivity of 80 m^2/s and an ultra-high seismogenic permeability of approximately 10^{-12} m^2 involving gas-rich (CO_2) fluids within a highly fractured medium (Talwani et al., 2007). According to these authors, a supra-hydrostatic fluid pressure of approximately 200 MPa at 10 km of depth developed within overpressurized traps, bounded by pre-existing structural and/or lithological discontinuities at the boundary between lower and upper crust. This overpressure is here interpreted as occurring just before

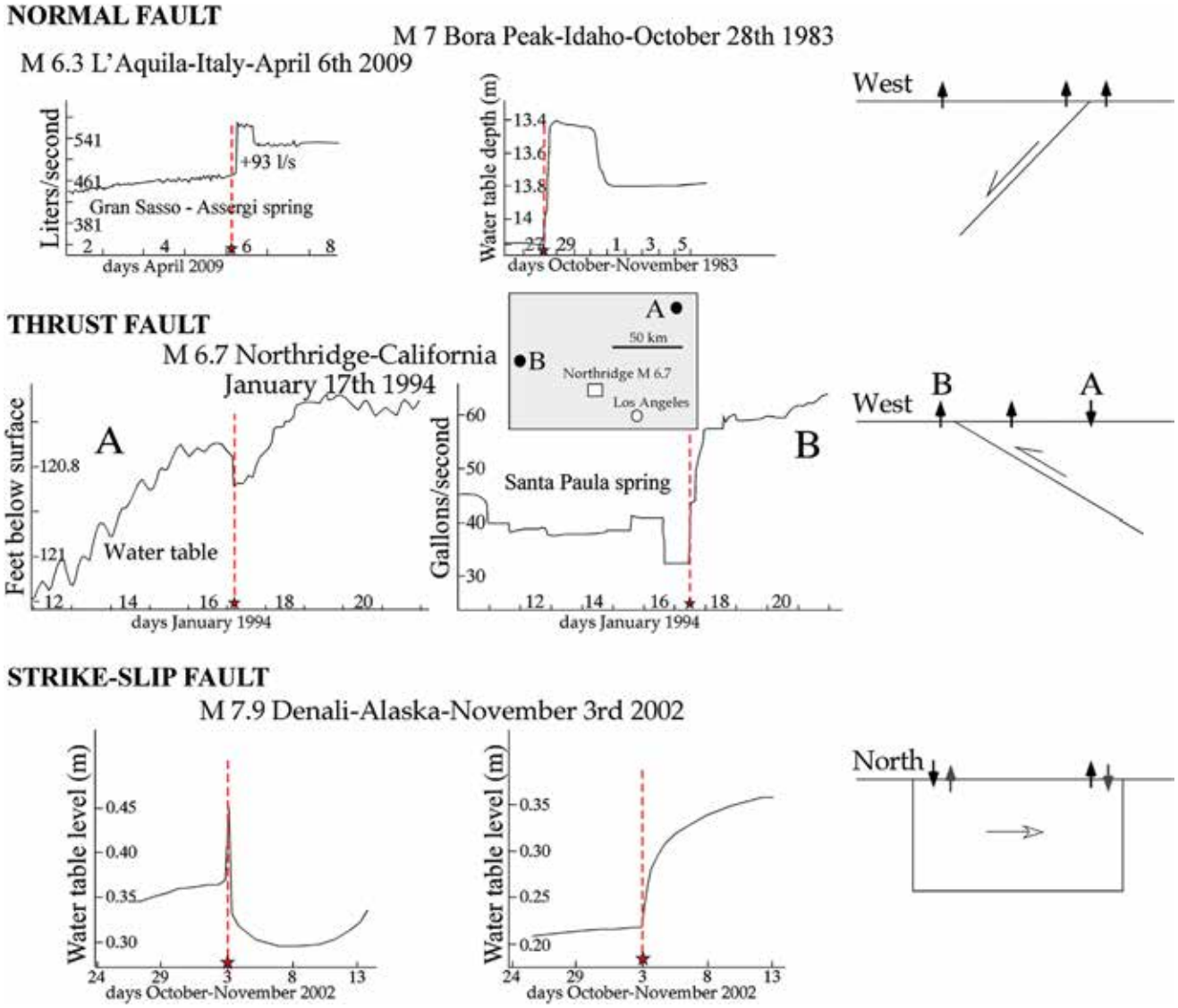

Figure 3. Examples of water changes during earthquakes. The L'Aquila-Italy, 2009 normal fault example illustrates an increase in water supply at a spring 14 km from the epicenter (Gran Sasso–Assergi) that began slowly days before the main event. An upraise of the water table was described during the Borah Peak-Idaho, 1983 normal fault-related earthquake. The thrust fault example (Northridge, 1994) shows a typical pattern of both lowering and upraising of the water table or discharge at springs. Along strike-slip faults a similar pattern occurs, with both uplift and lowering of the water level as evident for the Denali, 2002 event. The cross-sections to the right qualitatively illustrate the location of measurement with respect to the fault. In the strike-slip example, the rectangle simplifies the activated subvertical dextral strike-slip fault plane, and the water variations are in the eastern wall of the fault. Data of the L'Aquila 2009 event after courtesy of Gran Sasso S.p.A. Bora Peak Whitehead et al. (1985), Northridge, Sneed et al. (2003), Denali, Sil (2006).

Please cite this article in press as: Doglioni, C., et al., Fault on–off versus coseismic fluids reaction, Geoscience Frontiers (2013), http://dx.doi.org/10.1016/j.gsf.2013.08.004

the earthquake, induced by the initial fall of the fault hangingwall. Similar increase of fluids discharge has been reported for a number of past earthquakes in the southern Apennines, particularly for the M 6.9 November 23rd, 1980 event (Esposito et al., 2001). A dominant raise of the water table has been reported also for the M 7.3, Borah Peak, Idaho, October 28th, 1983 normal fault-related earthquake (Whitehead et al., 1985) (Fig. 3).

3.2. Thrust or reverse faults versus fluids

In compressive environments, fluids are primarily expelled during the interseismic stage (e.g., Oliver, 1986; Wannamaker et al., 2002). Mud volcanoes and gas hydrates along seismically quiet accretionary prisms testify this squeezing (e.g., Harris et al., 1998; Bonini, 2007). During the coseismic stage, the volume that was over-compressed during the interseismic period is dilated. Fractures open, releasing compressional stress at the BDT and resulting in a decrease of fluid pressure and possible percolation of fluids (Fig. 1). Both positive and negative variations in fluid discharge were observed during the thrust-related earthquakes in Chi-Chi 1999 (e.g., Chia et al., 2008). In some areas, positive and negative changes in the elevation of the water table were also observed. Another example is the Northridge 1994, M 6.7 thrust-related earthquake, in which there were both upraise of water discharge at springs about 50 km to the NW of the epicenter, along the strike of the thrust, and decline of the water table (Fig. 3) about 80 km to the NE (Sneed et al., 2003). The increase of water discharge was preceded, before the quake, by a decrease (Fig. 3). Relevant hydrologic changes have been observed with the Loma Prieta (California) 1989, M 7.1 earthquake (Rojstaczer and Wolf, 1992). A water level increase started three days before the 1985 M 6.1 Kettlemen Hill thrust-related earthquake in California. At the mainshock the water level dropped instantaneously, with a post-seismic slow recovery of the water table in the well (Roeloffs and Quilty, 1997). Stream-flow and ionic concentrations increased within 15 min after the earthquake. During the weeks to months following the event, the ground-water levels in the highland parts of the basin were lowered up to 21 m suggesting that the Loma Prieta earthquake increased rock permeability and temporarily enhanced groundwater flow in the region (Rojstaczer and Wolf, 1992).

May 20th and 29th 2012, in the Emilia salient at the leading edge of the northern Apennines accretionary prism buried beneath the Po Basin, two thrust-related Mw 6 and 5.9 earthquakes were preceded and followed by up to 8 m raise of the water table and temperature increase in wells located along the crest of the activated anticline.

Fluid-pressure cycles have been predicted to be out of phase in the ductile and brittle regimes along a thrust during the interseismic and coseismic stages by McCaig (1988). He also envisaged along shear zones the fluid flow to be episodic, and dominated by transient fracture permeability, being the evolution of micro-cracks different before and after the seismic rupture of a thrust. Greater degrees of connectivity among fractures and greater interseismic deformations result in a faster propagation of fluids during the coseismic stage.

3.3. Strike-slip faults versus fluids

Strike-slip related earthquakes also recorded at the same time both uplift and subsidence of the water table. Examples are the activated segments of right-lateral strike-slip faults during the Mw 6.5 June 17th and 21st 2000 events in Iceland, associated to the coseismic upraise and subsidence at the two tip lines, followed by opposite trends during post-seismic relaxation (Jonsson et al., 2003) and the M 7.2 right-lateral strike-slip fault related January 17th, 1995 Kobe earthquake in Japan (King et al., 1995; Tokunaga, 1999). Positive increase of the water table has been reported for the Parkfield seismicity in California (e.g., Roeloffs, 1998). Both upraise and decrease of the water table have been reported for the M 7.5 Denali, Alaska, November 3rd 2002 earthquake (Sil, 2006), as shown in Fig. 3.

The water table generally records the temperature of the host rocks. Because the depth of the water table may vary as a function of the stress change in the upper crust, depth changes cause thermal perturbations, which are potentially detectable by satellites (Quing et al., 1991; Tronin, 1996). During the days before the 1999 earthquake, temperatures increased along the Izmit Fault at the eastern tip line, as observed by radar analysis (Tramutoliet et al., 2005; Yürür, 2006). This variation is interpreted as associated with an uplift of the thermally stratified water table.

4. Numerical modeling

To evaluate the physical feasibility of the proposed geological interpretation (Figs. 1 and 2), and the observed fluid behavior in the different tectonic settings (Fig. 3), we modeled the interactions between fluids and rocks during the mechanics of faulting. Specifically, we investigated the fluid behavior during the interseismic and coseismic stages rather than addressing the processes controlling the timing of the rupture. Our models are intended as simplified general examples to show the feasibility of the above-described geological model. The regional application of our model to specific geological cases requires the further description of the fault plane, the medium composition and texture (including hydrological parameters), and specific boundary conditions.

Finite element dynamic modeling was performed using the commercial COMSOL Multiphysics 3.5 software (http://www.comsol.com/). Rock mechanics (plane strain or plane stress modules in COMSOL) and fluid behavior (Darcy's module) were solved contemporaneously (similarly to models available in the literature, e.g., Zhang et al., 2008). We adopted a poroelastic rheology with a Biot's coefficient equal to 1 (Young's Modulus: 2×10^{11} Pa; Poisson's Ratio: 0.33). Unlike Doglioni et al. (2011), the faults were treated as discrete rock volumes with a thickness of approximately 150 m (surfaces in the 2D geometry) instead of contact bodies (contact pairs in COMSOL's nomenclature). Preferential slip along the faults was obtained by imposing a smaller Young's Modulus with respect to the rest of the model. Unlocked sectors of the fault were modeled assuming a Young's Modulus of 5×10^9 Pa for thrust and normal faults and of 5×10^{10} Pa for strike slip faults, whereas locked portions were modeled assuming Young's modulus equal to 2×10^{11} Pa, i.e., equal to the remaining parts of the models. No convergence was obtained for smaller values in the unlocked sectors of the faults. However, the difference of Young's Moduli between the locked and unlocked sectors was enough to simulate slip.

Concerning fluid dynamics, the fluid Darcy's law was solved, and the fluid was assumed to be water with a density of 1000 kg m^{-3} and a viscosity of 0.0001 Pa s. The porosity and permeability of the rock were assumed, in our reference model, to be uniform (equal to 25% and 3×10^{-13} m^2 respectively). This is a common assumption in numerical modeling (e.g., Zhang et al., 2007), although permeability is expected to decrease with depth in the brittle layers of the crust and remain rather constant in the ductile layer (Manning and Ingebritsen, 1999; Ingebritsen and Manning, 1999; Bosl and Nur, 2002). The effects of varying permeability are discussed in the section dedicated to modeling results.

Also porosity is expected to decrease with depth and may be drastically reduced by mechanical and chemical compaction and veining (e.g., Deming, 1994). The choice of adopting a porosity equal to 25% typical of a sandstone at depths of 3–4 km, which will

Please cite this article in press as: Doglioni, C., et al., Fault on–off versus coseismic fluids reaction, Geoscience Frontiers (2013), http://dx.doi.org/10.1016/j.gsf.2013.08.004

lower to 10% at 6 km depth and to 5% at 10 km (Allen and Allen, 1990) is justified by the fact that we are interested in reproducing the behavior of the brittle portion of the crust. In igneous and metamorphic rock porosity is mainly controlled by fractures, which are far less predictable than primary porosity in sediments. A sensitivity analysis on the effects of variable porosity was performed. Negligible changes in the pattern of fluid movements were obtained for the porosity range 0.05–0.45. As the fluid velocities are concerned, maximum changes of ±26% were obtained at the surface for the same porosity interval. For this reason we decided to no complicate our model introducing variable porosity.

The velocities for the interseismic stage are shown as an average for the entire period (i.e., over 90 years). The velocities for the coseismic period are referred to the moment immediately after the occurrence of slip along the fault. In particular we show the difference between the coseismic velocity field and the velocity field at the last interseismic stage. The poroelastic effects of a quake are expected to disappear after some time (years, normally), and our choice is appropriate to show the change in water circulation from interseismic to coseismic periods, rather than investigating the decay of the effects of slip along the fault.

Doglioni et al. (2011) conducted a sensitivity analysis on the mechanical parameters adopted in the models for normal fault and thrust or reverse fault and concluded that the elastic constants (Young's modulus and Poisson's ratio) do not significantly affect the pattern of the stress field. For this reason, this type of sensitivity analysis of mechanical parameters was not performed in the present work. We instead discuss the effect of the variation of permeability on the velocity field predicted by the model.

Following Zhang et al. (2008), the permeability of rocks was varied, in some models, through time, according to the strain induced by deformation. The basic idea is that, where significant positive dilation occurs (i.e., volume gain), fractures induced by strain should enhance permeability, whereas negative dilation (i.e., rock contraction and volume loss) should close already existing fractures, decreasing permeability (e.g., Aydin, 2000). Dilation was calculated at each time step. In our simulations of normal and thrust or reverse fault, areas characterized by dilation values larger than 1.2×10^{-5} (volume gain) were assigned a permeability 1.5×10^{-12} m^2 (factor 5 increase) or alternatively of 3×10^{-12} m^2 (factor 10 increase), whereas areas characterized by dilation smaller than -1.2×10^{-5} (volume loss) were assigned a permeability of 1.5×10^{-14} m^2 (factor 5 decrease) or alternatively of 3×10^{-14} m^2 (factor 10 decrease). The dilation threshold values proposed are not experimentally supported. In principle the variation of the permeability during interseismic stages could be linear (or follow different laws) with increase of dilation. Since we are mostly concerned with the fluid behavior at the transition from the interseismic to coseismic stage, our assumption can be considered adequate. In models of strike-slip fault, areas characterized by dilation values larger than 0.1×10^{-5} (volume gain) were assigned a permeability of 1.5×10^{-12} m^2 or alternatively of 3×10^{-12} m^2, whereas areas characterized by dilation smaller than -0.1×10^{-5} (volume loss) were assigned a permeability of 1.5×10^{-14} m^2 or alternatively of 3×10^{-14} m^2. Of course, in nature a continuous variation of permeability with dilation changes is expected to occur, rather than an instantaneous change at dilation thresholds. A change of such threshold values would increase or decrease the area of the model characterized by permeability changes and thus increase or reduce the permeability-change effects that will be described later. However, the choice of uniform parameters allows describing the effect of permeability changes on the first order pattern of fluid flow rather than constraining the velocity of fluid migration and the details of fluid flow pattern. A further step should be brought forth in order to describe specific rather than general cases. In all the models, the permeability of the stick-slip portions of the faults was turned from 3×10^{-13} m^2 at interseismic stages to 3×10^{-12} m^2 at coseismic stages, to simulate the opening of fractures during fault slip. Finally, also the adopted geometry of faults is a simplification of reality. In all the modeled cases, the faults are straight lines, although undulations are typically observed in nature. In addition, normal and thrust faulting crossing the brittle-ductile transition could be characterized by listric geometry. The planar shape was chosen to keep the problem simple and investigate the effect of the different behavior of rocks across the brittle-ductile transition for normal and thrust faults and at the boundary between locked and unlocked segments for strike-slip faults. Undulations of fault surfaces would lead to local variations of the state of stress, as widely discussed by Carminati and Vadacca (2010).

4.1. Normal and thrust faults

As modeling dedicated to normal and thrust fault is concerned, a 2D-plane strain approximation was adopted to couple the mechanics of fault with fluid behavior. Plane strain is chosen because it is normally used to model geological processes in 2D described by vertical cross sections. For thrust and normal fault, the simple geometry of the model was taken from Doglioni et al. (2011), who solved only the mechanical problem. Fig. 4a and b illustrates the simple model geometry and boundary conditions. The model was 20 km deep and 42 km wide and was separated in two distinct parts by a 45° dipping plane to simulate both normal fault or thrust earthquakes, the behavior (locked or unlocked) of which varies in space and time. The finite element grid was composed of 9716 triangular linear Lagrange elements (59,115 degrees of freedom). The deeper (>9 km) portion of the thrust and normal faults was modeled as always unlocked to simulate the ductile (aseismic) slip of faults at depth.

Gravity was applied as a body force to all of the elements. A uniform density (2850 kg m^{-3}) and gravity acceleration was set (9.81 m s^{-2}).

Permeability changes, if any, were applied only in the brittle layer of models dedicated to thrust and normal fault, in the assumption that the absence of fracturing in ductile layers should prevent significant changes of permeability.

As thrust or reverse and normal faults are concerned, the fluid-dynamics boundary conditions (Fig. 4b) included no flux/symmetry for all of the boundaries except for the surface boundary, modeled as a free surface (atmosphere). Modeling was performed in three separate stages. At first, a pre-stress model was used, applying gravity. During this stage, the following boundary conditions were applied: only horizontal slip was allowed along the lower boundary. Only vertical slip was allowed along the lateral boundaries, and the surface was left free. The free-slip boundary condition at the bottom simulated the slip over a horizontal detachment of crustal blocs. This assumption is justified by the fact that at a depth of 20 km, the crust is expected to behave plastically. Assuming other boundary conditions along the lower boundary, such as applying Winkler forces, did not affect the results in the portion of the model that is of interest. During this modeling stage, the seismogenic portion of the fault (i.e., in the 0–9 km range) was left unlocked.

In a second stage, a displacement of 0.9 m (directed to the left for normal fault and to the right for thrust fault) was imposed in 9 time steps of 10 years each to the left boundary of the model. The remaining boundary conditions were unvaried. The seismogenic portion of the fault was locked to simulate the stress accumulation during the interseismic period of the seismic cycle. In a third stage, at a time equal to 100 years, the seismogenic fault was unlocked,

Please cite this article in press as: Doglioni, C., et al., Fault on–off versus coseismic fluids reaction, Geoscience Frontiers (2013), http://dx.doi.org/10.1016/j.gsf.2013.08.004

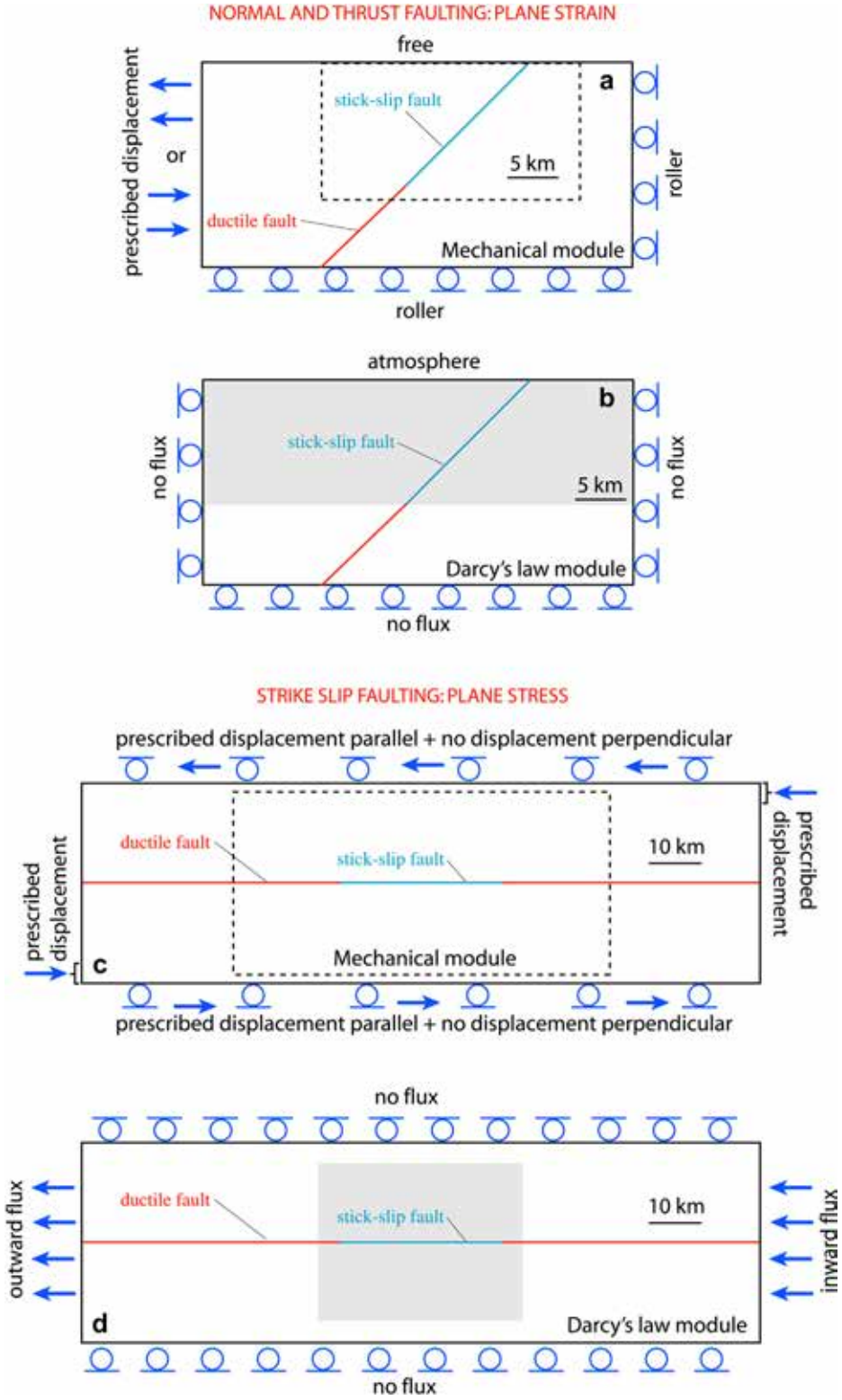

Figure 4. The geometry and boundary conditions for the numerical models of thrust and normal faults (a, b) and strike slip faults (c, d) are shown. In the gray areas, variations of the permeability were allowed, as described in the text. The dashed rectangles indicate the parts of the models shown in Figs. 5–7.

and 0.1 m of additional displacement (for a total displacement of 1 m) was imposed to the left boundary of the model to simulate the coseismic stress field. In our model, rupture was imposed a priori, via a change of the Young's Modulus in the brittle portion of the fault, because a self-consistent failure criterion was not assumed. On average, the 1 m stretching and shortening applied at the model boundary generated slip of about 17 cm in the stick-slip portion of the fault at the coseismic stage.

Figs. 5 and 6 illustrate the velocity fields predicted for the fluids by numerical models simulating normal and thrust or reverse

Please cite this article in press as: Doglioni, C., et al., Fault on–off versus coseismic fluids reaction, Geoscience Frontiers (2013), http://dx.doi.org/10.1016/j.gsf.2013.08.004

faults. Fig. 7 shows the dilation predicted by the models at interseismic and coseismic stages. For a discussion on the stress field predicted by the models, the reader is referred to the work of Doglioni et al. (2011). Figs. 5a and 6a show the results for our reference model, in which permeability was kept constant (3×10^{-13} m^2) throughout the model for the entire simulation. In this case, fluid flow velocities are primarily a function of gradients in fluid pore pressures. Consistently with theoretical expectations, normal fault was characterized by generalized downward motion of fluids during the preseismic stages (Fig. 5a), but upward motion was predicted during the coseismic stage (Fig. 5b) for the area to the left of the fault. Additionally, the area directly above the fault was associated with localized downward motion of the fluids. Thrust fault was associated with generalized upward motion during the interseismic stage (Fig. 6) and by downward motion during the coseismic stage (Fig. 6). Decreasing the Biot's coefficient to 0.5, the model predicted velocities half of those predicted by our reference model.

If permeability is varied according to strain changes, as in panels b and c of Figs. 5 and 6, the fluid velocity field is controlled both by gradients in fluid pore pressures and permeability changes, the latter becoming more important with the increase of the imposed change. Figs. 5b and 6c show the fluid velocity field for normal fault when permeability is increased, in strongly dilated volumes (where dilation is larger than 1.2×10^{-5}), by a factor 5 or 10 respectively. Such volumes (bordered by the thick purple lines in the figures) develop during the interseismic stage. Models characterized by a larger increase in permeability predict progressively larger flux of fluids towards these volumes. At the coseismic stage this dilated volume returns to smaller dilation values and permeability is reduced to the reference value. As a consequence, fluids are expulsed from this rock volume. These results are consistent with our hypothetical model. Although not shown in figures, simulations were performed increasing the amount of interseismic displacement at the model boundaries. Increasing the boundary displacement enlarges the areas affected by permeability changes for both

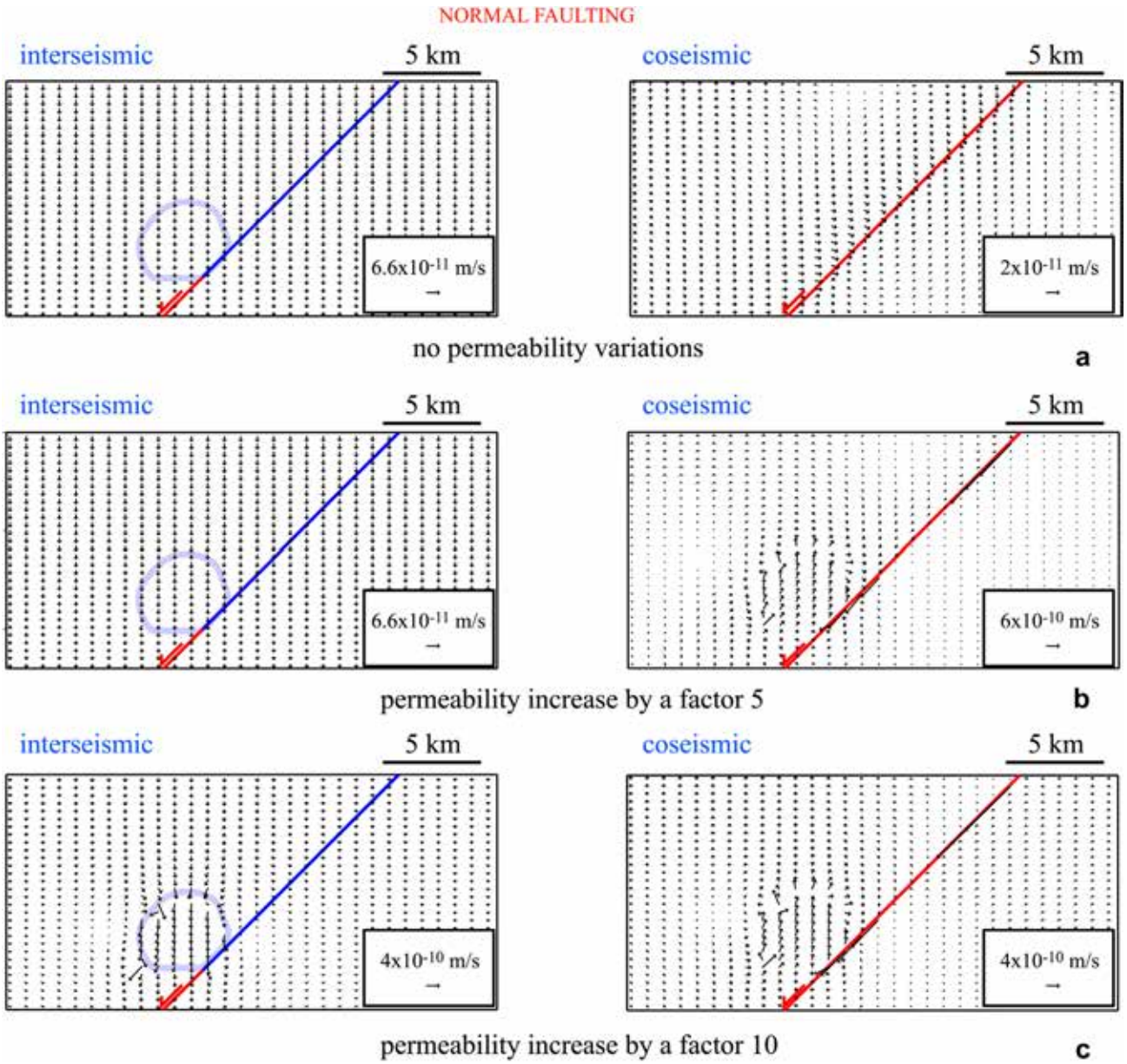

Figure 5. Fluid velocity field predicted for a normal faulting during interseismic and coseismic stages. In panel (a) no permeability changes were allowed (reference model). In panels (b) and (c), strongly dilated areas (indicated by the blue thick line) were respectively associated with a permeability 5–10 times larger than in the reference model.

Please cite this article in press as: Doglioni, C., et al., Fault on–off versus coseismic fluids reaction, Geoscience Frontiers (2013), http://dx.doi.org/10.1016/j.gsf.2013.08.004

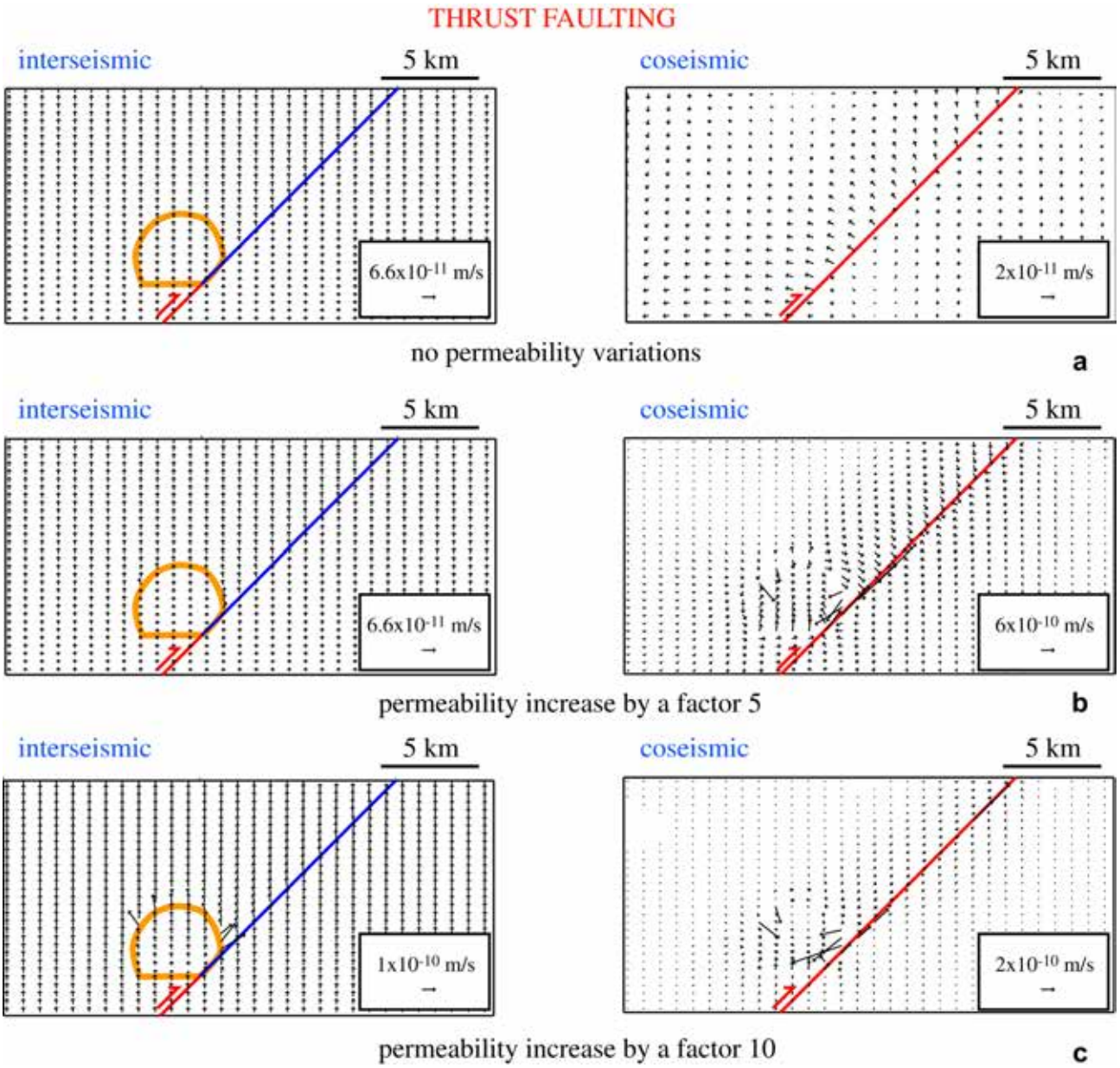

Figure 6. Fluid velocity field predicted for a thrust faulting during interseismic and coseismic stages. In panel (a) no permeability changes were allowed (reference model). In panels (b) and (c), strongly contractional areas (indicated by the orange thick line) were respectively associated with a permeability 5–10 times smaller than in the reference model.

normal and thrust fault models, issuing in an even larger flux. Fig. 6b and c shows the fluid velocity field for thrust or reverse fault when permeability is decreased, in strongly contractional volumes (where dilation is smaller than -1.2×10^{-5}), by a factor 5 or 10 respectively. Once again, such volumes (bordered by the thick orange lines in the figures) develop during the interseismic stage. At the coseismic stage this contractional volume returns to higher dilation values and permeability is increased back to the reference value. Consistently with the hypothetical model, fluids are deviated away from such volumes during interseismic stages and converge towards them in coseismic stages.

Fig. 8 shows the vertical component of velocity of the fluids at the surface (in the model domain shown in Figs. 5 and 6) at interseismic and coseismic stages. As normal fault is considered, all the models predict, at the interseismic stage, overall downward motion (negative velocities), consistently with the predictions of the hypothetical model. The regular downward motion of the model with no permeability variations is perturbed when permeability changes are forced, but the general pattern for the three models is similar. At the coseismic stage, the model without permeability changes predicts upward motion of the fluids only in the left half of the shown domain, whereas in the models with forced permeability changes the area characterized by upward motion is larger and gets closer to the fault. As suggested by our hypothetical model, all the numerical models predict a drastic change in the fluid velocity field at the surface, but the models characterized by permeability changes are more consistent with the theoretical expectations.

As thrust or reverse fault is concerned (Fig. 8b), all the models predict, at the interseismic stage, overall upward motion (with some perturbations in the models with permeability changes), consistently with the predictions of the hypothetical model. At the

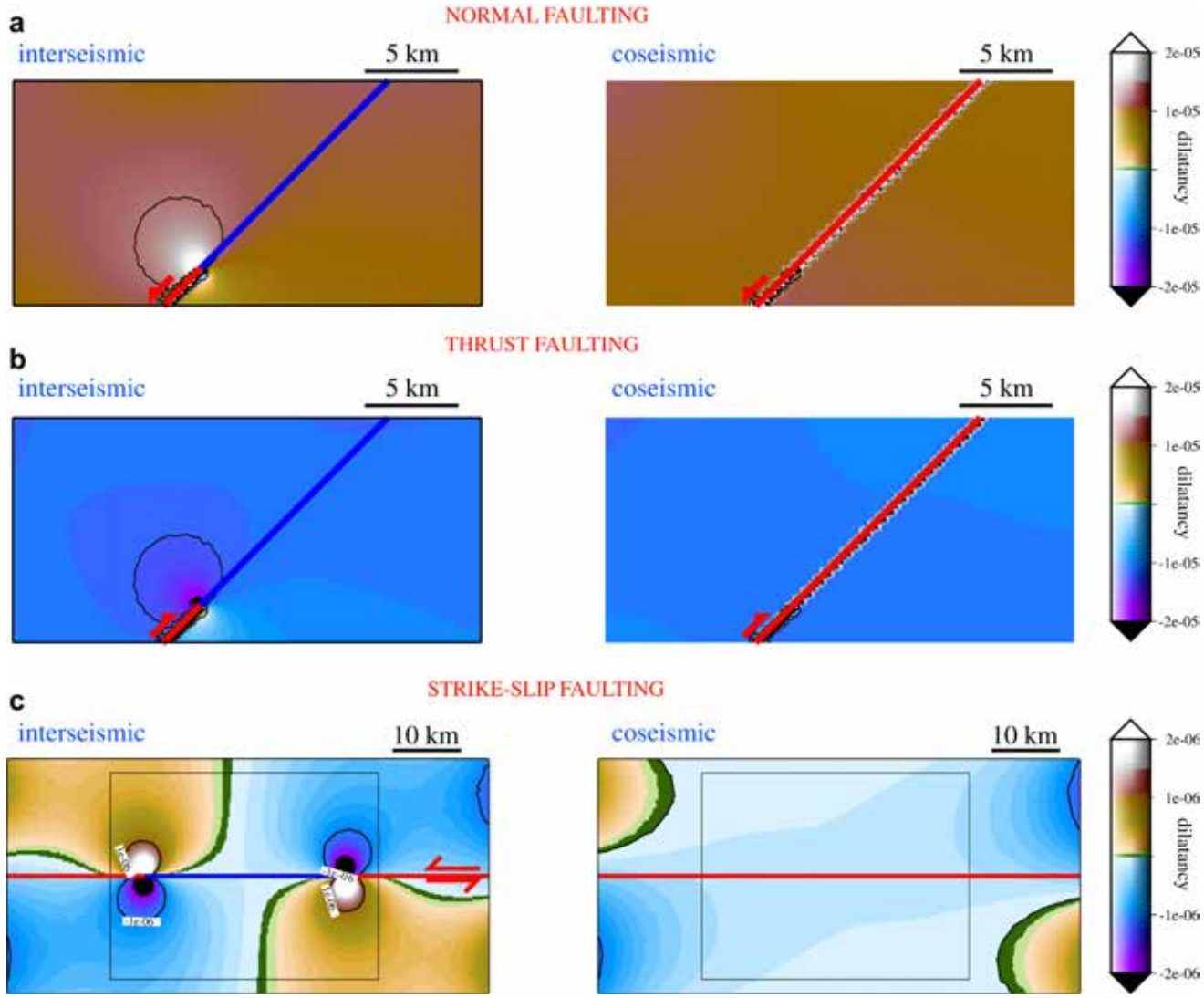

Figure 7. Dilation predicted by the numerical models at interseismic and coseismic stages for normal (a), thrust (b) and strike-slip (c) faults. The dilation is referred to models in which the permeability was changed by a factor 10 in strongly contractional or dilational areas, indicated by the black circular lines. Very similar patterns are predicted also by the models in which no change or a factor 5 change was applied. In panel (c), the black rectangle shows the area in which the permeability changes were applied. In panels (a) and (b), permeability changes were limited to the fault and to the brittle layer (at depths shallower than 10 km).

coseismic stage, the model without permeability changes predicts downward motion of the fluids only in the left half of the domain, whereas in the models with forced permeability changes downward motion occurs closer to the fault. Model predictions are fairly consistent with the theoretical expectations and with the natural cases.

4.2. Strike-slip fault

For strike-slip fault, a plane stress approximation was adopted. Plane stress is chosen because it is normally used to model in 2D geological processes in map view. The geometry adopted for strike-slip fault is shown in Fig. 4b. In this case, our purpose is to model the effect of the existence of locked and unlocked (aseismic slip) segments of the fault on the stress field and on fluid behavior rather than simulating brittle and ductile behavior across the brittle-ductile transition. The model is 130 km long and 38 km wide and is separated in two distinct parts by an E-W fault plane. The finite element grid was composed of 18,784 triangular linear Lagrange elements (113,307 degrees of freedom). The central part of the strike-slip fault is locked during the interseismic period and unlocked at coseismic time. The remaining parts are always left unlocked, to simulate aseismic creep.

In models of strike-slip fault, the permeability changes were applied to the central part of the model (see Fig. 4d) since the dilation registered close to the right and left boundaries is induced by boundary effects, rather than by real geological processes. The fluid dynamics boundary conditions included no flux/symmetry for the upper and lower boundaries. An inward flux at a rate of 1×10^{-11} m/s was imposed at the right edge of the model, whereas an outward flux at the same speed was imposed to the left edge (Fig. 4d). These boundary conditions generated a regional flux of water toward the left. Assuming no regional flux (e.g., by imposing no flux/symmetry to all the model boundaries) allows very low fluid velocities and generates instable solutions, controlled by local numerical perturbations. The condition of regional flux helps showing how permeability changes affect the regional flux at the tip points of the stick-slip portion of the fault. In a first stage, a displacement of 0.9 m (directed to the left on the top and right-top sides of the model and directed to the right along the bottom and

Please cite this article in press as: Doglioni, C., et al., Fault on–off versus coseismic fluids reaction, Geoscience Frontiers (2013), http://dx.doi.org/10.1016/j.gsf.2013.08.004

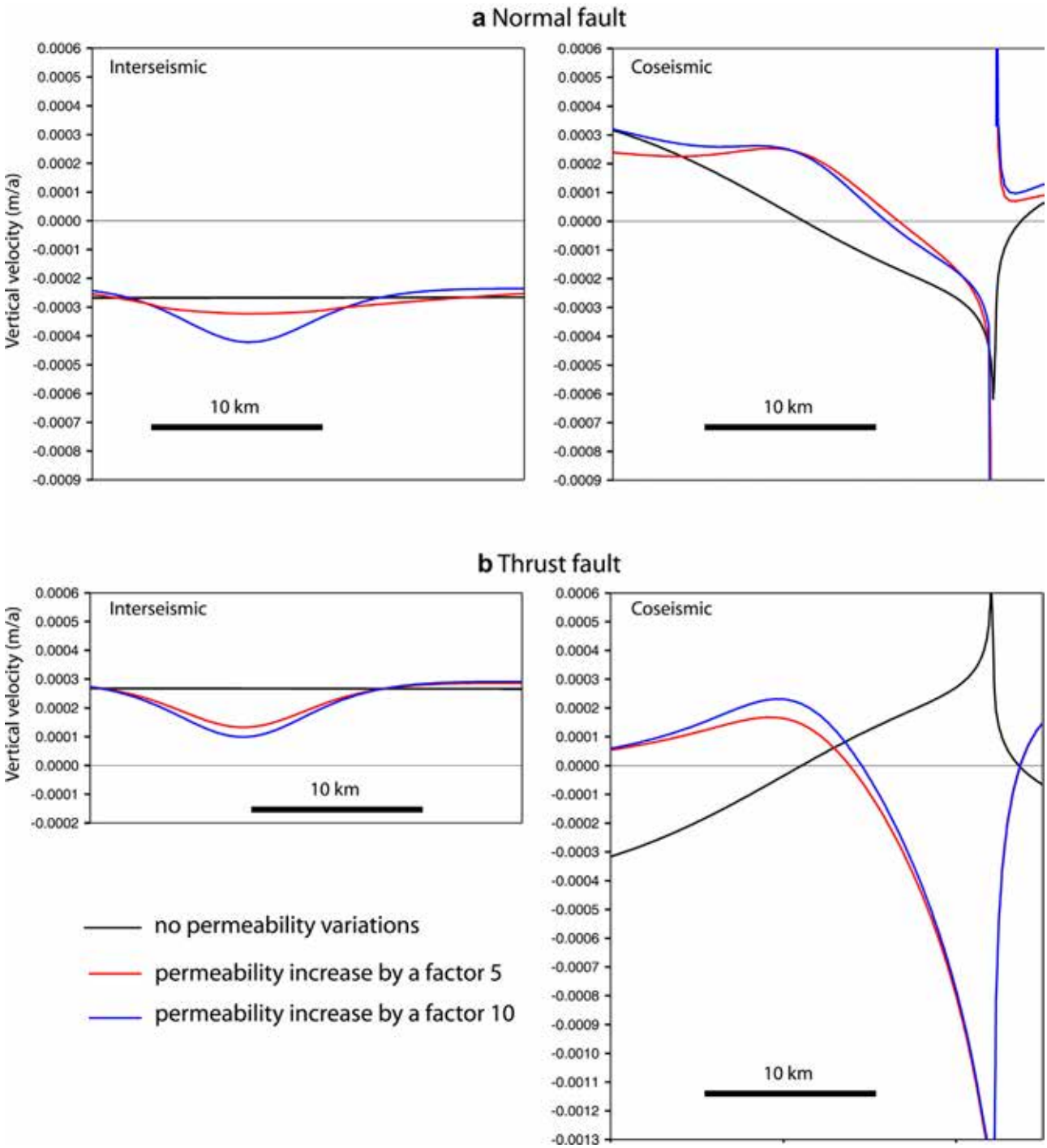

Figure 8. Vertical component of the fluid velocity predicted by models of normal (a) and thrust (b) faulting at interseismic and coseismic stages. The results are shown for the same model domain of Figs. 4 and 5. Positive velocities indicate upward motion.

bottom-left sides) was imposed in 9 time steps of 10 years each to the left boundary of the model. In addition, no motion perpendicular to the model boundary was imposed to the top and bottom sides. The remaining boundary conditions are left free. The seismogenic portion of the fault was locked to simulate the stress accumulation during the interseismic period of the seismic cycle. In a second stage, at a time equal to 100 years, the seismogenic fault was unlocked, and 0.1 m of additional displacement on both bottom and top sides was imposed to the left boundary of the model to simulate the coseismic stress field, while the seismogenic part of the fault was unlocked. The displacement boundary conditions simulate a total left-lateral slip of 2 m along the boundaries over 100 years. Owing to the elastic deformation of the model, only 10 cm of displacement occur in the stick-slip portion of the fault at the coseismic stage. This justifies why a lower dilation threshold was adopted for strike-slip fault than for normal and thrust faults.

Fig. 9a shows the results for our reference model, in which permeability was kept constant (3×10^{-13} m^2) throughout the model for the entire simulation. Fig. 7c shows the dilation predicted

by the strike-slip models at interseismic and coseismic stages. Coupled and anti-symmetric "strongly" dilated (dilation larger than 0.1×10^{-5}) and "strongly" contractional (dilation smaller than -0.1×10^{-5}) pairs develop at the two tip points of the locked fault, consistently with the hypothetical model of Fig. 2, the only difference being the shape of the dilated and contractional areas (circular in the numerical modeling and wedge shaped in the hypothetical model). Such difference is due to the adopted rheology. Zhang et al. (2008) showed that, assuming elasto-plastic rheology, cuspate shaped dilational bands are predicted by numerical models of strike-slip fault. This observation can be applied also to the results for normal and thrust or reverse fault. Fig. 8a shows that, if permeability is kept constant, no changes in the imposed regional flow of fluids are observed. In addition, the velocity changes induced by the coseismic slip are very minor (notice that the scale is greatly changed with respect to that of the interseismic stage), for constant permeability.

Fig. 9b and c shows that, if permeability changes are forced in strongly dilated and contractional volumes, the fluid velocity field is deviated in correspondence of the tip points of the stick-slip portion of the strike-slip fault. In particular, during interseismic stages fluid flow is deviated toward the dilated volumes and away from contractional volumes, characterized by larger and smaller permeability respectively. Since dilated and contractional volumes disappear during the coseismic stage, a contrary fluid pattern is predicted, with fluids escaping the formerly dilated volumes and entering the formerly contractional volumes. These predictions are consistent with the hypothetical model shown in Fig. 2.

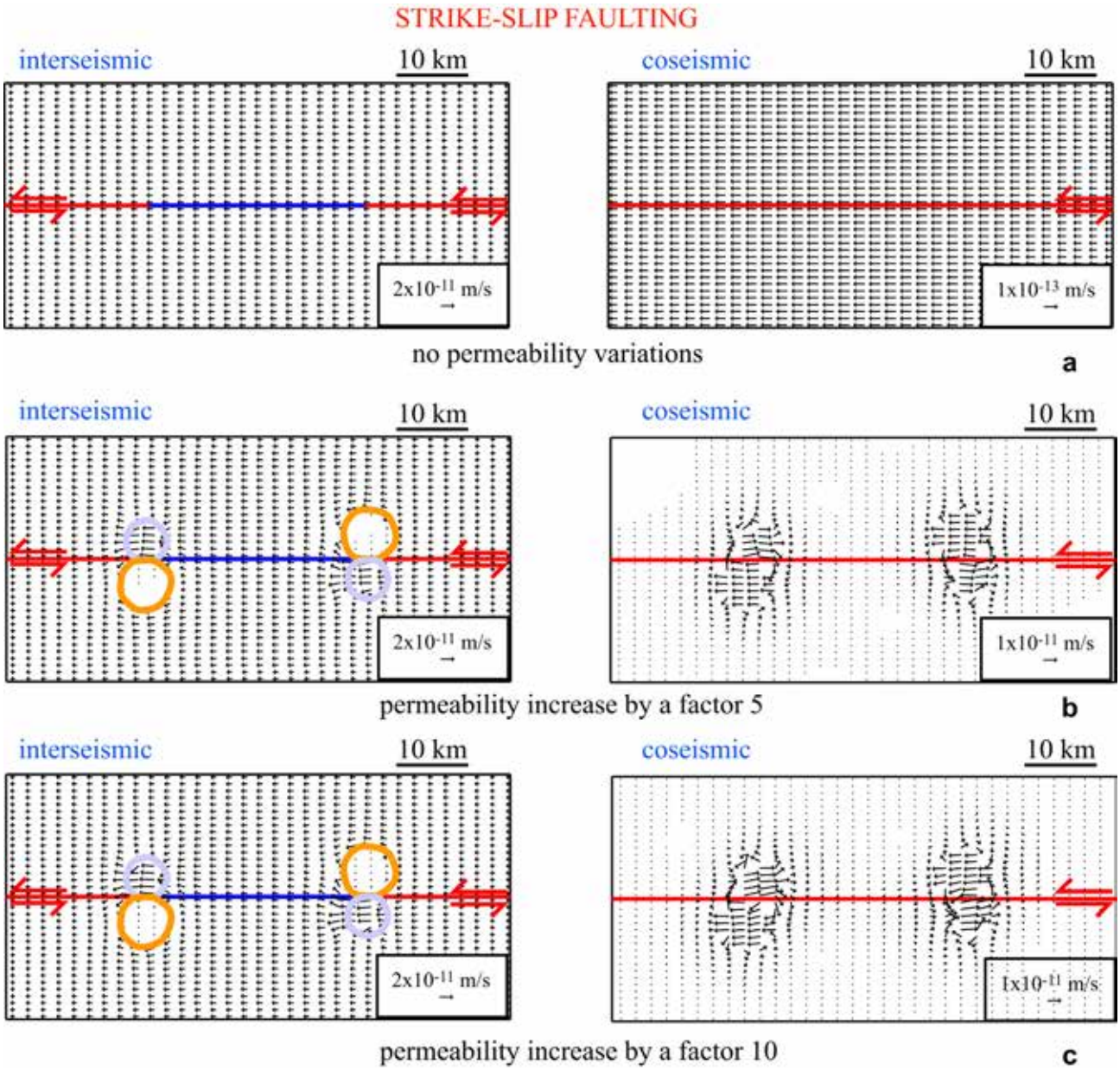

Figure 9. Fluid velocity field predicted for a strike-slip faulting during interseismic and coseismic stages. In panel (a) no permeability changes were allowed (reference model). In panels (b) and (c), strongly contractional areas (indicated by the orange thick line) were respectively associated with a permeability 5–10 times smaller than in the reference model; strongly dilated areas (indicated by the blue thick line) were respectively associated with a permeability 5–10 times larger than in the reference model.

Please cite this article in press as: Doglioni, C., et al., Fault on–off versus coseismic fluids reaction, Geoscience Frontiers (2013), http://dx.doi.org/10.1016/j.gsf.2013.08.004

5. Discussion

Our model represents a first-order simplification, which includes two layers, one BDT, and one fault that is either fully locked or fully unlocked. Because the lithosphere and crust are lithologically heterogeneous, more than one BDT may develop, and several acquicludes may be present at different levels. Moreover, other mechanisms neglected here, such as the presence of multiple asperities or the variability of the friction along the fault plane, make the system unstable and affect the "locked-unlocked" behavior of fault segments. However, adding more complexity yields the same logic when we consider the interseismic and coseismic stages as end-members without the time evolution. The consequent simplified reaction of fluids is hypothetically shown in Figs. 5 and 6. During the interseismic period the fluids are expected to migrate into the areas subject to dilation, whereas fluids should be slowly expelled from the volumes of rocks under contraction. Since the three main tectonic settings have different relationship of dilation/compression, we infer that the fluids react accordingly. For example, along a normal fault, the fluids accumulated into cracks during the interseismic period or even shallow acquifers are squeezed out during the coseismic stage characterized by opposite contraction (Fig. 1). The passage of seismic waves may also contribute to significant oscillations of the water table. Along a strike-slip fault, the locked parts of the fault should correspond to a shear zone in the deeper ductile layer (Fig. 2). Along the active, creeping segments of the fault, the brittle crust is better coupled to (and moving together with) the deeper ductile crust, although the coupling may be a transient phenomenon (Cakir et al., 2005). The locked brittle segment should be associated with stretching and shortening at the two tip lines during the interseismic stage. These two rock volumes are characterized by a reversal in polarity of the stress field during the coseismic stage (Fig. 2), which leads to opposite flow directions of the fluids at the margins of the activated strike-slip fault.

In all tectonic settings, the opening and closing bands form parallel to the σ_2 stress tensor. They invert during the coseismic stage. Fluid discharge varies as a function of the tectonic style during the interseismic and coseismic stage.

6. Conclusions

In our model, the pattern of dilation and contraction in strained rocks during interseismic and coseismic stages depends on the tectonic setting. In all cases, the BDT was relevant in controlling fault activation and fluid flow, ultimately determining the seismic cycle. In the interseismic stage, we assumed a constant slip rate in the ductile fault segment, and locking in the upper brittle segment. From this model, the following main conclusions were drawn:

(1) The stress distribution generated at the BDT during the interseismic period yields (a) dilation (crack opening and increase of secondary porosity) at the base of locked normal faults and (b) contraction (crack closure and decrease of secondary porosity) at the base of locked thrusts.
(2) Fluid discharge of opposite sign is expected during preseismic (i.e., weak discharge along normal faults and large along thrusts) and coseismic (i.e., discharge increase along normal faults and a decrease along thrusts) periods (Fig. 1).
(3) In the coseismic stage of strike-slip fault (Fig. 2), the motion reverses along the two subvertical bands located at the fault tips and that were already deformed during the interseismic stage (i.e., the band in tension experienced coseismic compression, and the band in compression experienced coseismic tension). Therefore, fluids should be expelled from the frontal coseismic compressive tip lines of the strike-slip fault whereas, at the opposite end tips, fluids should be transported to depth (Fig. 2).

Numerical modeling (Figs. 4–9) and the regional examples (Fig. 3) support the influence of the BTD as one of the possible mechanisms for controlling the evolution of the seismic cycle and the role of fluids. The pre-seismic stage (e.g., Fig. 1) may show anomalies useful for possible short term alert system. This suggests that the combination of tectonic setting studies, associated with GPS, strain rate (e.g., Riguzzi et al., 2012), fluid discharge and related thermal and electrical conductivity transients can help to develop a physical basis for future time-dependent earthquake hazard studies.

Acknowledgments

We thank Edie Miglio and Giuliano Panza for fruitful discussions. Comments and suggestions by the Editor M. Santosh, Ron Harris and an anonymous reviewer were very helpful. This research benefited from funding provided by the Italian Presidenza del Consiglio dei Ministri – Dipartimento della Protezione Civile (DPC) within the INGV-DPC 2007–2009 agreement (Project S1), Sapienza University and CNR-Eurocores-TopoEurope. Diana is thanked for delaying her birth, allowing her father (EC) to conclude numerical modeling.

References

Adinolfi, F.R., Falgiani, A., Manetta, M., Marchetti, A., Parisse, B., Petaccia, R., Petitta, M., Rusi, S., Sciannamblo, D., Spizzico, M., Tallini, M., 2009. Hydrogeological and Hydrogeochemical Effects on the Gran Sasso Carbonate Groundwater Due to the L'Aquila Earthquake (April 6, 2009). Geoitalia, Rimini.

Allen, P.A., Allen, J.R., 1990. Basin Analysis: Principles and Applications. Blackwell Scientific Publications, Cambridge, 451 pp.

Amoruso, A., Crescentini, L., Petitta, M., Rusi, S., Tallini, M., 2011. Impact of the 6 April 2009 L'Aquila earthquake on groundwater flow in the Gran Sasso carbonate aquifer. Central Italy. Hydrological Processes 25, 1754–1764. http://dx.doi.org/10.1002/hyp.7933.

Aydin, A., 2000. Fractures, faults, and hydrocarbon entrapment, migration and flow. Marine and Petroleum Geology 17, 797–814.

Bodvarsson, G., 1970. Confined fluids as strain meters. Journal of Geophysical Research 75, 2711–2718.

Bonini, M., 2007. Interrelations of mud volcanism, fluid venting, and thrust-anticline folding: examples from the external northern Apennines (Emilia-Romagna, Italy). Journal of Geophysical Research 112, B08413. http://dx.doi.org/10.1029/2006JB004859.

Bosl, W.J., Nur, A., 2002. Aftershocks and pore fluid diffusion following the 1992 Landers earthquake. Journal of Geophysical Research 107 (B12), 2366.

Cakir, Z., Akoglu, A.M., Belabbes, S., Ergintav, S., Meghraoui, M., 2005. Creeping along the Ismetpasa section of the North Anatolian fault (Western Turkey): rate and extent from InSAR convection. Earth and Planetary Science Letters 238, 225–234. http://dx.doi.org/10.1016/j.epsl.2005.06.044.

Carminati, E., Vadacca, L., 2010. 2D and 3D numerical simulations of the stress field at the thrust-front of the Northern Apennines, Italy. Journal of Geophysical Research 115, B12425. http://dx.doi.org/10.1029/2010JB007870.

Cattin, R., Avouac, J.P., 2000. Modeling mountain building and the seismic cycle in the Himalaya of Nepal. Journal of Geophysical Research 105 (B6), 13,389–13,407.

Chia, Y., Chiu, J.J., Chiang, Y.-H., Lee, T.-P., Liu, C.-W., 2008. Spatial and temporal changes of groundwater level induced by thrust faulting. PAGEOPH 165, 5–16.

Cox, S.F., 1995. Faulting processes at high fluid pressures – an example of fault valve behavior from the Wattle Gully Fault, Victoria, Australia. Journal of Geophysical Research 100, 12841–12859.

Deming, D., 1994. Fluid flow and heat transport in the upper continental crust. In: Parnell, J. (Ed.), Geofluids: Origin, Migration and Evolution of Fluids in Sedimentary Basins, Geological Society Special Publication, vol. 78, pp. 27–42.

Di Luccio, F., Ventura, G., Di Giovambattista, R., Piscini, A., Cinti, F.R., 2010. Normal faults and thrusts re-activated by deep fluids: the 6 April 2009 Mw 6.3 L'Aquila earthquake, central Italy. Journal of Geophysical Research 115 (B06315), 15. http://dx.doi.org/10.1029/2009JB007190.

Doglioni, C., Barba, S., Carminati, E., Riguzzi, F., 2011. Role of the brittle-ductile transition on fault activation. Physics of the Earth and Planetary Interiors 184, 160–171. http://dx.doi.org/10.1016/j.pepi.2010.11.005.

Eichhubl, P., Boles, J.R., 2000. Focused fluid flow along faults in the Monterey Formation, coastal California. Geological Society of America Bulletin 112 (11), 1667–1679.

Esposito, E., Pece, R., Porfido, S., Tranfaglia, G., 2001. Hydrological anomalies connected to earthquakes in southern Apennines (Italy). Natural Hazards and Earth System Sciences 1, 137–144 (European Geophysical Society).

Harris, R.A., Sawyer, R.K., Audley-Charles, M.G., 1998. Collisional melange development: geologic associations of active melange-forming processes with exhumed melange facies in the western Banda orogen, Indonesia. Tectonics 17 (3), 458–480.
Hobbs, B., Ord, A., 1988. Plastic instabilities: implications for the origin of intermediate and deep focus earthquakes. Journal of Geophysical Research 93, B9. http://dx.doi.org/10.1029/JB093iB09p10521.
Ingebritsen, S.E., Manning, C.E., 1999. Geological implications of a permeability-depth curve for the continental crust. Geology 27, 1107–1110.
Italiano, F., Martinelli, G., Bonfanti, P., Caracausi, A., 2009. Long-term (1997–2007) geochemical monitoring of gases from the Umbria-Marche region. Tectonophysics. http://dx.doi.org/10.1016/j.tecto.2009.02.040.
Jonsson, S., Segall, P., Pedersen, R., Bjornsson, G., 2003. Post-earthquake ground movements correlated to pore-pressure transients. Nature 424, 179–183. http://dx.doi.org/10.1038/nature01776.
Kanamori, H., Anderson, D.L., 1975. Theoretical basis of some empirical relations in seismology. Bulletin of the Seismological Society of America 65, 1073–1095.
King, C.-Y., Koizumi, N., Kitagawa, Y., 1995. Hydrogeochemical anomalies and the 1995 Kobe Earthquake. Science 269 (5220), 38–39. http://dx.doi.org/10.1126/science.269.5220.38.
Lucente, F.P., De Gori, P., Margheriti, L., Piccinini, D., Di Bona, M., Chiarabba, C., Piana Agostinetti, N., 2010. Temporal variation of seismic velocity and anisotropy before the 2009 Mw 6.3 L'Aquila earthquake, Italy. Geology 38 (11), 1015–1018. http://dx.doi.org/10.1130/G31463.1.
Manga, M., Wang, C.-Y., 2007. Earthquake hydrology. In: Schubert, G. (Ed.), Treatise on Geophysics, vol. 4 (10), pp. 293–320.
Manning, C.E., Ingebritsen, S.E., 1999. Permeability of the continental crust: implications of geothermal data and metamorphic systems. Reviews of Geophysics 37, 127–150.
Marone, C., 1998. Laboratory-derived friction laws and their application to seismic faulting. Annual Review of Earth and Planetary Sciences 26, 643–696.
Matsumoto, N., Takahashi, M., 1994. State space modeling to detect changes of ground water level associated with earthquakes. In: Paper Presented at IUGG XXI General Assembly, International Union of Geodesy and Geophysics, Boulder, Colorado.
Matthäi, S.K., Fischer, G., 1996. Quantitative modeling of fault-fluid-discharge and fault-dilation-induced fluid-pressure variations in the seismogenic zone. Geology 24, 183–186.
McCaig, A.M., 1988. Deep fluid circulation in fault zones. Geology 16, 867–870.
Meade, B.J., Hager, B.H., 2005. Block models of crustal motion in southern California constrained by GPS measurements. Journal of Geophysical Research 110, B03403. http://dx.doi.org/10.1029/2004JB003209.
Micklethwaite, S., Cox, S.F., 2004. Fault-segment rupture, aftershock-zone fluid flow, and mineralization. Geology 32, 813–816. http://dx.doi.org/10.1130/g20559.1.
Miller, S.A., Nur, A., Olgaard, D.L., 1996. Earthquakes as a coupled shear stress high pore pressure dynamical system. Geophysical Research Letters 23, 197–200.
Miller, S.A., Nur, A., 2000. Permeability as a toggle switch in fluid-controlled crustal processes. Earth and Planetary Science Letters 183, 133–146.
Miller, S.A., 2002. Properties of large ruptures and the dynamical influence of fluids on earthquakes and faulting. Journal of Geophysical Research 107. http://dx.doi.org/10.1029/2000jb000032, 2182.
Miller, S., Collettini, C., Chiaraluce, L., Cocco, M., Barchi, M.R., Kohl, T., 2004. Aftershock driven by a high pressure CO_2 source at depth. Nature 427, 724–727.
Muir-Wood, R., King, G.C.P., 1993. Hydrological signatures of earthquake strain. Journal of Geophysical Research 98 (B12), 22,035–22,068.
Oliver, J., 1986. Fluids expelled tectonically from orogenic belts: their role in hydrocarbon migration and other geologic phenomena. Geology 14, 99–102. http://dx.doi.org/10.1130/0091-7613(1986)14.
Panza, G.F., La Mura, C., Peresan, A., Romanelli, F., Vaccari, F., 2012. Seismic hazard scenarios as preventive tools for a disaster resilient society. In: Dmowska, R. (Ed.), Advances in Geophysics. Elsevier, pp. 93–165.
Peresan, A., Kossobokov, V., Romashkova, L., Panza, G.F., 2005. Intermediate-term middle-range earthquake predictions in Italy: a review. Earth-Science Reviews 69, 97–132.
Peresan, A., Panza, G.F., 2012. Improving earthquake hazard assessments in Italy: an alternative to "Texas Sharpshooting". EOS 93, 538–539.
Pingue, F., De Natale, G., 1993. Fault mechanism of the 40 seconds subevent of the 1980 Irpinia (Southern Italy) earthquake from levelling data. Geophysical Research Letters 20 (10), 911–914.
Plastino, W., Panza, G.F., Doglioni, C., Frezzotti, M.L., Peccerillo, A., De Felice, P., Bella, F., Povinec, P.P., Nisi, S., Ioannucci, L., Aprili, P., Balata, M., Cozzella, M.L., Laubenstein, M., 2011. Uranium groundwater anomalies and active normal faulting. Journal of Radioanalytical and Nuclear Chemistry 288, 101–107.
Quing, Z., Xiu-Deng, X., Chang-Gong, D., 1991. Thermal infrared anomaly – precursor of impending earthquakes. Chinese Science Bulletin 36, 319–323.
Riguzzi, F., Crespi, M., Devoti, R., Doglioni, C., Pietrantonio, G., Pisani, A.R., 2012. Geodetic strain rate and earthquake size: new clues for seismic hazard studies. Phys Earth Planet Inter 206–207, 67–75.
Roeloffs, E.A., 1988. Hydrologic precursors to earthquakes: a review. Pure and Applied Geophysics 126, 177–209.
Roeloffs, E.A., 1998. Persistent water level changes in a well near Parkfield, California, due to local and distant earthquakes. Journal of Geophysical Research 103, 869–889.
Roeloffs, E., Quilty, E., 1997. Water level and strain changes preceding and following the August 4, 1985 Kettleman Hills, California, earthquake. Pure and Applied Geophysics 149, 21–60.
Rojstaczer, S., Wolf, S., 1992. Permeability changes associated with large earthquakes: an example from Loma Prieta, California. Geology 20, 211–214.
Rudnicki, J.W., Yin, J., Roeloffs, E.A., 1993. Analysis of water level changes induced by fault creep at Parkfield, California. Journal of Geophysical Research 98, 8143–8152.
Ruina, A., 1983. Slip instability and state variable friction laws. Journal of Geophysical Research 88, 10359–10370.
Salazar, J.M.L., Perez, N.M., Hernandez, P.A., Soriano, T., Barahona, F., Olmos, R., Cartagena, R., Lopez, D.L., Lima, R.N., Melian, G., Galindo, I., Padron, E., Sumino, H., Notsu, K., 2002. Precursory diffuse carbon dioxide degassing signature related to a 5.1 magnitude earthquake in El Salvador, Central America. Earth and Planetary Science Letters 205, 81–89.
Savage, J.C., 1983. A dislocation model of strain accumulation and release at a subduction zone. Journal of Geophysical Research 88, 4984–4996.
Sibson, R.H., 1981. Controls on low-stress hydro-fracture dilatancy in thrust, wrench and normal fault terrains. Nature 289, 665–667.
Sibson, R.H., 1992. Implications of fault-valve behaviour for rupture nucleation and recurrence. Tectonophysics 211, 283–293.
Sibson, R.H., 2000. Fluid involvement in normal faulting. Journal of Geodynamics 29, 469–499. http://dx.doi.org/10.1016/S0264-3707(99)00042-3.
Sibson, R.H., Moore, J.Mc.M., Rankin, A.H., 1975. Seismic pumping-a hydrothermal fluid transport mechanism. Journal of the Geological Society 131 (6), 653–659. http://dx.doi.org/10.1144/gsjgs.131.6.0653.
Sieh, K., Natawidjaja, D.H., Meltzner, A.J., Shen, C.-C., Cheng, H., Li, K.-S., Suwargadi, B.W., Galetzka, J., Philibosian, B., Edwards, R.L., 2008. Earthquake supercycles inferred from sea-level changes recorded in the Corals of West Sumatra. Science 322 (5908), 1674–1678. http://dx.doi.org/10.1126/science.1163589.
Sil, S., 2006. Response of Alaskan Wells to Near and Distant Large Earthquakes (Master thesis). University of Alaska Fairbanks, pp. 1–83.
Slejko, D., Caporali, A., Stirling, M., Barba, S., 2010. Occurrence probability of moderate to large earthquakes in Italy based on new geophysical methods. Journal of Seismology 14, 27–51. http://dx.doi.org/10.1007/s10950-009-9175-x.
Sneed, M., Galloway, D.L., Cunningham, W.L., 2003. Earthquakes-rattling the Earth's Plumbing System. USGS Fact Sheet 096-03, pp. 1–5.
Talwani, P., Chen, L., Gahalaut, K., 2007. Seismogenic permeability, ks. Journal of Geophysical Research 112, B07309. http://dx.doi.org/10.1029/2006JB004665.
Tenthorey, E., Cox, S.F., Todd, H.F., 2003. Evolution of strength recovery and permeability during fluid-rock reaction in experimental fault zones. Earth and Planetary Science Letters 206, 161–172.
Terakawa, T., Zoporowski, A., Galvan, B., Miller, S.A., 2010. High-pressure fluid at hypocentral depths in the L'Aquila region inferred from earthquake focal mechanisms. Geology 38, 995–998. http://dx.doi.org/10.1130/G31457.1.
Thatcher, W., 1993. The earthquake cycle and its role in the long-term deformation of the continental lithosphere. Annali di Geofisica 36, 13–24.
Thatcher, W., Rundle, J.B., 1979. A model for the earthquake cycle in underthrust zones. Journal of Geophysical Research 84, 5540–5556.
Tramutoli, V., Cuomo, V., Filizzola, C., Pergola, N., Pietrapertosa, C., 2005. Assessing the potential of thermal infrared satellite surveys for monitoring seismically active areas. The case of Kocaeli (Izmit) earthquake, August 17th, 1999. Remote Sensing of Environment 96, 409–426.
Tronin, A.A., 1996. Satellite thermal survey – a new tool for the studies of seismoactive regions. International Journal of Remote Sensing 17, 1439–1455.
Tokunaga, T., 1999. Modeling of earthquake-induced hydrological changes and possible permeability enhancement due to the 17 January 1995 Kobe Earthquake, Japan. Journal of Hydrology 223, 221–229.
Tullis, J., Yund, R.A., Farver, J., 1996. Deformation-enhanced fluid distribution in feldspar aggregates and implications for ductile shear zones. Geology 24, 63–66.
Wakita, H., 1996. Geochemical challenge to earthquake prediction. Proc. Natl. Acad. Sci. U. S. A. 93, 3781–3786.
Wannamaker, P.E., Jiracek, G.R., Stodt, J.A., Caldwell, T.G., Porter, A.D., Gonzalez, V.M., McKnight, J.D., 2002. Fluid generation and pathways beneath an active compressional orogen, the New Zealand Southern Alps, inferred from magnetotelluric (MT) data. Journal of Geophysical Research 107. ETG 6, 1–ETG 6, 20.
Whitehead, R.L., Harper, R.W., Sisco, H.G., 1985. Hydrologic changes associated with the October 28, 1983, Idaho earthquake. Pure and Applied Geophysics 122 (2–4), 280–293. http://dx.doi.org/10.1007/BF00874599.
Yürür, M.T., 2006. The positive temperature anomaly as detected by Landsat TM data in the eastern Marmara Sea (Turkey): possible link with the 1999 Izmit earthquake. International Journal of Remote Sensing 27 (6), 1205–1218.
Zhang, Y., Lin, G., Wang, Y.J., Roberts, P.A., Ord, A., 2007. Numerical modelling of deformation and fluid flow in the Shui-Kou-Shan mineralisation district, Hunan Province, South China. Ore Geology Reviews 31, 261–278.
Zhang, Y., Schaubs, P.M., Zhao, C., Ord, A., Hobbs, B.E., Barnicoat, A.C., 2008. Fault-related dilation, permeability enhancement, fluid flow and mineral precipitation patterns: numerical models. Geological Society, London, Special Publications 299, 239–255.

Please cite this article in press as: Doglioni, C., et al., Fault on–off versus coseismic fluids reaction, Geoscience Frontiers (2013), http://dx.doi.org/10.1016/j.gsf.2013.08.004